Journal of Advanced Electronic Materials
http://dx.doi.org/10.62762/JAEM.2026.128242

RESEARCH ARTICLE

Effect of Assisted Sintering Temperature on the Structural, Dielectric, and Magnetic Properties of $BaK_{1-x}Na_xGd_3Fe_5O_{15}$ Tetragonal Tungsten Bronze Ceramics

Syeda Mahnoor Fatima[1,*], **Fayaz Hussain**[1,*], **Shehreen Nadeem**[1], **Muhammad Fahad Riaz**[2], **Sajida Sheikh**[1], **Yasemin Tabak**[3] and **Atilla Evcin**[4]

[1] Department of Materials Engineering, NED University of Engineering & Technology, Karachi 75270, Pakistan
[2] Department of Metallurgy and Materials Engineering, Dawood University of Engineering and Technology, Karachi 74800, Pakistan
[3] TUBITAK National Metrology Institute (UME), Gebze, Kocaeli 41470, Turkey
[4] Materials Science and Engineering Department, Afyon Kocatepe University, Afyonkarahisar 032004, Turkey

Abstract

A series of non-stoichiometric $BaK_{1-x}Na_xGd_3Fe_5O_{15}$ ($x = 0.00$, 0.10, 0.20, 0.30) tetragonal tungsten bronze (TTB) ceramics were synthesized via solid-state reaction, cold sintering at 150 °C, and assisted sintering at 400 °C and 500 °C. XRD confirmed single-phase TTB formation. Enhanced crystallinity and sharper diffraction peaks with increasing assisted sintering temperature indicated improved grain growth and ordering. Density measurements revealed Na^+ substitution combined with salt-assisted processing significantly influenced densification, with BKGF-1NST$_2$ achieving the highest bulk density of 4.32 g/cm^3. Dielectric characterization showed frequency-dependent behavior with decreasing loss at higher frequencies, while selected compositions exhibited stable dielectric response after 500 °C assisted sintering. Magnetic measurements confirmed ferrimagnetic behavior via Fe^{3+}-mediated interactions. BKGF-2NT$_2$ ($x = 0.20$, assisted sintered at 500 °C) delivered optimal magnetic performance: $M_s = 4.97$ emu g^{-1}, $M_r = 1.59$ emu g^{-1}, $H_c = 1435.84$ Oe, attributed to optimized exchange interactions, improved crystallinity, and enhanced grain connectivity. Co-doping with cold-assisted sintering governs the structural, dielectric, and magnetic properties of TTB ceramics.

Keywords: tetragonal tungsten bronze, cold-assisted sintering, magnetic property, dielectric, particle size.

Submitted: 10 June 2026
Revised: 24 July 2026
Accepted: 25 July 2026
Published: 19 August 2026

Vol. 2, **No.** 3, 2026.
10.62762/JAEM.2026.128242

***Corresponding authors:**
✉ Syeda Mahnoor Fatima
fatimamahnoor923@gmail.com
✉ Fayaz Hussain
fhussain@neduet.edu.pk

Citation
Fatima, S. M., Hussain, F., Nadeem, S., Riaz, M. F., Sheikh, S., Tabak, Y., & Evcin, A. (2026). Effect of Assisted Sintering Temperature on the Structural, Dielectric, and Magnetic Properties of $BaK_{1-x}Na_xGd_3Fe_5O_{15}$ Tetragonal Tungsten Bronze Ceramics. *Journal of Advanced Electronic Materials*, 2(3), 101–112.

1 Introduction

Multiferroic materials, which exhibit more than one ferroic order, such as ferroelectricity, ferromagnetism, or ferroelasticity, have attracted increasing attention due to their potential use in multifunctional applications, including non-volatile memories, magnetoelectric sensors, and spintronic devices [1–4]. These materials exhibit spontaneous electric and magnetic polarization, typically reflected through hysteresis loops when exposed to external fields [5, 6]. However, despite extensive research, very few multiferroic compounds exhibit robust room-temperature functionality. Among them, $BiFeO_3$ remains one of the most cited; although A-site substitution such as Ba doping can partially improve its magnetic and ferroelectric response, its intrinsic antiferromagnetic behavior and weak magnetoelectric coupling still pose significant limitations [2, 5, 7].

To address these challenges, attention has shifted from conventional perovskite-type structures to alternative frameworks like tetragonal tungsten bronze (TTB), which offer higher structural flexibility [2, 4, 5]. The TTB structure, generally formulated as $A_2BC_2M_5O_{15}$, accommodates five different cationic sites, thus enabling more extensive chemical substitution than the perovskite lattice [5, 6, 8]. This flexibility has opened pathways for tailoring multiferroic behavior through site-specific doping. Notable TTB-based systems such as $Sr_xBa_{1-x}Nb_2O_6$ and $Ba_2NaNb_5O_{15}$ have been extensively studied for their ferroelectric and relaxor properties, while recent works have demonstrated that magnetic cations like Fe^{3+} when substituted into the TTB lattice or coexisting phases, can induce room-temperature magnetic ordering [2, 5, 8–10].

In iron-containing TTB systems, both isovalent and aliovalent substitution at the A-site can significantly influence lattice distortion, oxygen vacancy concentration, magnetic exchange interactions, and dielectric polarization mechanisms. Incorporation of alkali ions such as Na^+ modifies local structural symmetry and affects charge compensation behavior, as demonstrated in alkali-modified niobate systems where varying K/Na ratios systematically alter structural symmetry and functional properties [11], while rare-earth ions such as Gd^{3+} may contribute to enhanced magnetic ordering and stabilization of the TTB framework. Previous studies on tungsten bronze ceramics have demonstrated that Na-based compositional substitution can effectively tailor dielectric relaxation and energy storage performance through structural and defect engineering [12, 13]. In addition, magnetic anisotropy and multifunctional response in iron-containing TTB systems can be tuned through site-specific doping and lattice modification [14, 15]. However, comparatively limited work has been reported on Gd and Na modified iron-containing TTB ceramics processed using low-temperature cold sintering routes, particularly in systems combining cold sintering with assisted post-sintering treatment.

Meanwhile, traditional ceramic synthesis methods often require high-temperature sintering (>1000 °C), which leads to high embodied energy and substantial carbon emissions. For instance, the ceramic industry contributes approximately 41 Tg of CO_2 annually due to firing processes [16, 17]. Furthermore, most reported TTB multiferroic ceramics are fabricated using conventional sintering temperatures above 1000 °C, which often result in alkali volatilization, abnormal grain growth, secondary phase formation, and increased energy consumption [16, 18–20].

The combination of cold sintering with moderate assisted sintering offers a potential alternative approach for achieving sufficient densification while preserving compositional homogeneity and controlling grain evolution. Assisted sintering at intermediate temperatures may additionally improve crystallinity, grain connectivity, and magnetic ordering without requiring the extremely high temperatures associated with conventional ceramic processing [21–24]. Therefore, understanding the influence of assisted sintering temperature on the dielectric and magnetic response of Na-modified TTB ceramics remains scientifically important for the development of energy-efficient multifunctional materials.

The cold sintering process (CSP) has recently emerged as an energy-efficient alternative for fabricating oxide ceramics at significantly reduced temperatures compared with conventional solid-state sintering [14, 19, 22–25]. In CSP, a transient liquid phase combined with uniaxial pressure enables dissolution–precipitation assisted mass transport, particle rearrangement, and localized diffusion at temperatures generally below 300 °C [16, 18, 19]. This approach minimizes alkali volatilization, suppresses exaggerated grain growth, and reduces thermal stresses that are commonly observed during high-temperature processing of TTB ceramics [14, 19, 22–24]. However, cold-sintered ceramics may still exhibit incomplete crystallization and limited grain connectivity due to insufficient thermal activation. Therefore, assisted sintering at moderate temperatures can provide additional atomic diffusion and structural ordering while preserving the energy-saving advantages of CSP. Although considerable progress has been made in the development of tetragonal tungsten bronze ceramics and low temperature sintering techniques, studies on $BaK_{1-x}Na_xGd_3Fe_5O_{15}$ ceramics processed by cold-assisted sintering remain limited. In particular, the influence of assisted sintering temperature on the structural evolution and its correlation with the dielectric and magnetic properties of Na-substituted TTB ceramics has not been thoroughly investigated. Therefore, further study is required to understand how composition and assisted sintering conditions together influence the multifunctional properties of these ceramics.

In the present work, $BaK_{1-x}Na_xGd_3Fe_5O_{15}$ ($x = 0.00$, 0.10, 0.20, 0.30) tetragonal tungsten bronze ceramics were fabricated by cold-assisted sintering followed by assisted sintering at 400 °C and 500 °C. The effects of Na^+ substitution and assisted sintering temperature on the phase formation, density, dielectric behavior, and magnetic properties were systematically evaluated. The results demonstrate an effective low-temperature processing route for improving the multifunctional characteristics of TTB ceramics while reducing the thermal budget compared with conventional sintering.

2 Materials and Methods

$BaCO_3$ (>99%, Sigma-Aldrich), K_2CO_3 (>99%, Sigma-Aldrich), Na_2CO_3 (>99%, Sigma-Aldrich), Gd_2O_3 (>99.9%, Sigma-Aldrich), and Fe_2O_3 (>99%, Sigma-Aldrich) were selected as starting materials. All powders were preheated at 400 °C for 3 hours in a muffle furnace to eliminate moisture and reduce contamination. The pre-dried materials were then weighed according to the non-stoichiometric formula $BaK_{1-x}Na_xGd_3Fe_5O_{15}$, where $x = 0.00$, 0.10, 0.20, and 0.30 (BKGF, BKGF-1N, BKGF-2N, and BKGF-3N). Isovalent dopants were introduced at the A-site to investigate the influence of varying sodium concentration on thermal, magnetic, and dielectric properties.

The weighed powders were mixed and ground using a planetary ball mill with zirconia media in the presence of ethanol for 2 hours to promote homogeneity and reduce particle size. The resulting slurry was dried and calcined at 800 °C for 3 hours with a heating rate of 10 °C/min to ensure phase development and removal of volatile compounds. A second round of milling was conducted for 2 hours with ethanol to further refine the grain size and enhance surface area. The powders were then dried at 80 °C, sieved, and subjected to particle size analysis using a Laser Particle Analyzer (Model No. BT-9300H). The analyzer, equipped with a 3 mW semiconductor laser diode ($\lambda = 635$ nm), measured particle size over a duration of 1 to 3 minutes, using water as the immersion liquid. Pellets of 12.7 mm diameter and ∼1 g weight were prepared using a hydraulic press.

For comparative analysis, samples were fabricated both with and without the addition of a salt binder. Cold sintering was carried out at 150 °C while assisted sintering was carried out at 400 °C and 500 °C to investigate densification behavior under assisted sintering conditions. The assisted sintering temperatures of 400 °C and 500 °C were selected based on previous cold-assisted sintering studies together with preliminary optimization experiments, which indicated that this temperature range provides sufficient thermal energy to improve crystallinity, grain-boundary diffusion, and densification while maintaining the advantages of low-temperature processing and minimizing alkali volatilization. Phase composition and crystallographic information were obtained using an X-ray diffractometer (PANalytical X'Pert Pro, Netherlands) at room temperature with Cu-Kα radiation ($\lambda = 1.5406$ Å), operated at 40 kV and 30 mA over a 2θ range of 10°–80°. Data were analyzed using HighScore Plus software with PDF-4+ (2022) database and Rietveld refinement. Electrical and dielectric properties, including capacitance, inductance, and resistance, were measured using an LCR meter (Model Tonghui TH 2826) across a frequency range of 1 Hz to 5 MHz and temperatures up to 400 °C. Prior to measurement, silver paste was applied to both surfaces of the pellets to ensure proper electrical contact. The dielectric constant (ε_r) was calculated using the equation:

$$\varepsilon_r = \frac{C_p \times t}{\varepsilon_0 \times A}$$

where C_p is the capacitance, t is the pellet thickness, A is the electrode area, and ε_0 is the permittivity of free space (8.854×10^{-12} F/m). Magnetic measurements were performed using a Vibrating Sample Magnetometer (VSM, MicroSense Model No. 1660 MRS, USA), and M-H hysteresis loops were recorded to study the magnetic behavior of the synthesized ceramics. The density and volume

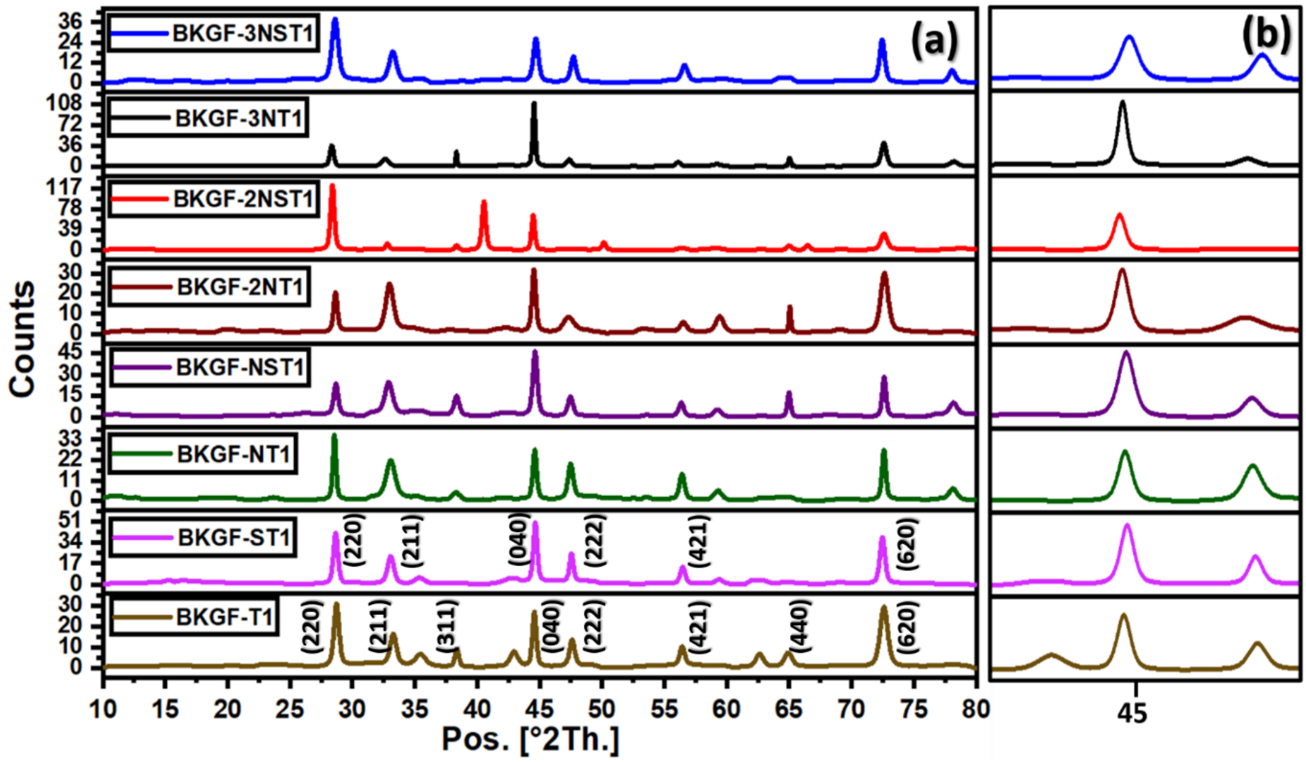

Figure 1. XRD patterns of sintered compositions of $BaK_{1-x}Na_xGd_3Fe_5O_{15}$ ($x = 0.10, 0.20, 0.30$) at 400 °C. (b) Enlarged view of the 45° (2θ) peak.

of all compositions (BKGF, BKGF-1N, BKGF-2N, and BKGF-3N), with and without salt binder, were measured using the Archimedes method.

During the cold sintering process, deionized water was used as a transient liquid medium to facilitate dissolution–reprecipitation mechanisms under applied pressure and moderate temperature. The slightly acidic nature of deionized water, resulting from dissolved atmospheric CO_2, assists in partial surface dissolution of alkali-containing species such as K^+ and Na^+, thereby enhancing ionic mobility, particle rearrangement, and neck formation between ceramic particles [16, 19]. This transient liquid phase promotes densification at significantly lower temperatures compared with conventional sintering routes [19, 25]. In addition to deionized water processing, selected samples were prepared using salt-assisted treatment to investigate its influence on densification and functional behavior.

The presence of dissolved ionic species in salt water can modify interfacial diffusion kinetics, enhance ionic transport, and influence grain-boundary chemistry during assisted sintering. Such effects may improve particle packing and local mass transport, thereby affecting density, dielectric response, and magnetic ordering. Furthermore, salt-assisted processing may alter defect distribution and oxygen vacancy concentration, which are known to strongly influence dielectric relaxation and magnetic exchange interactions in iron-containing TTB ceramics.

In this study for sample identification, N denotes Na-doped compositions, T1 and T2 represent assisted sintering at 400 °C and 500 °C, respectively, S indicates processing using salt water instead of deionized water, and the combination NS denotes Na-doped samples processed using the salt-water medium.

3 Results and Discussion

X-ray diffraction (XRD) patterns of $BaK_{1-x}Na_xGd_3Fe_5O_{15}$ ceramics sintered at 400 °C and 500 °C are presented in Figures 1 and 2, respectively. All compositions exhibit a prominent diffraction peak near 45° (2θ), confirming the formation and stability of the tetragonal tungsten bronze (TTB) structure. The persistence of the major diffraction peaks across all sodium concentrations and processing conditions indicates that the fundamental TTB framework remains structurally stable despite compositional modifications. Similar structural stability has been reported in related TTB ferroelectric and dielectric systems [2, 8, 26].

The experimental diffraction patterns were indexed

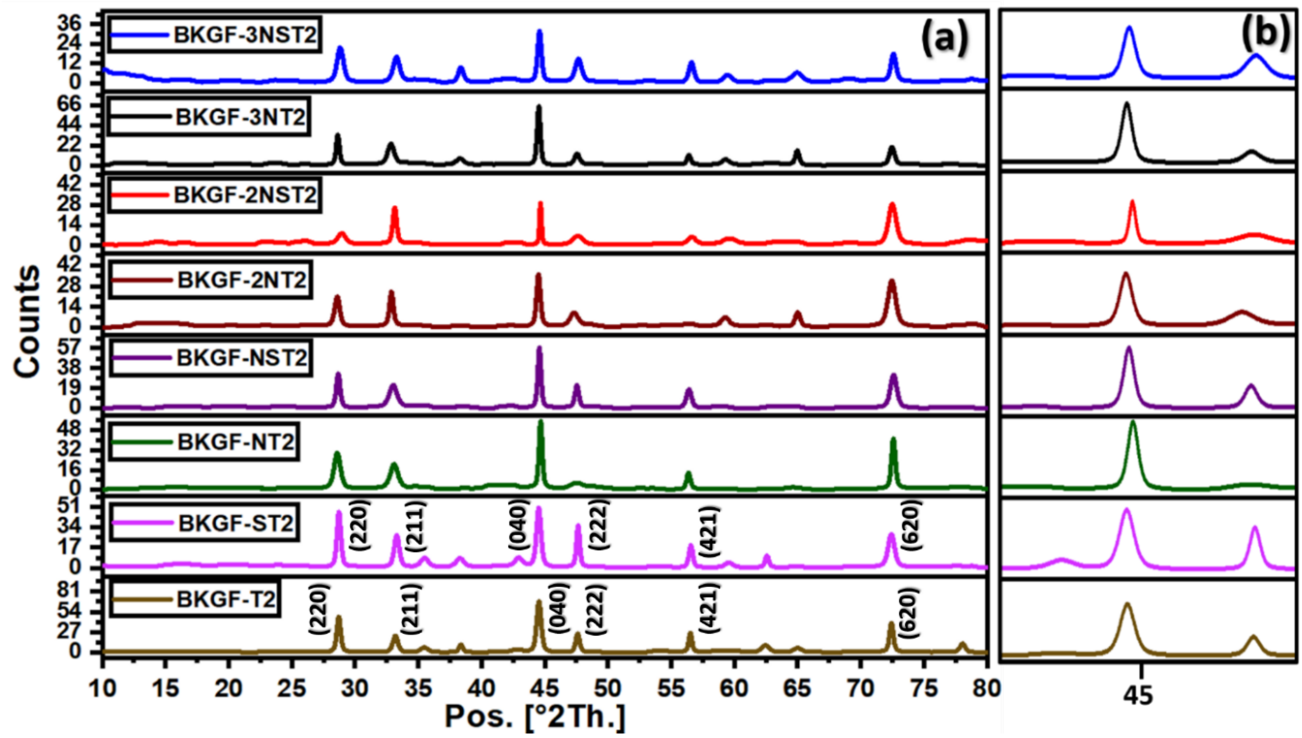

Figure 2. XRD patterns of sintered compositions of $BaK_{1-x}Na_xGd_3Fe_5O_{15}$ ($x = 0.10, 0.20, 0.30$) at 500 °C. (b) Enlarged view of the 45° (2θ) peak.

using the crystallographic information provided by ICDD PDF Card No. 01-085-1748, while theoretical crystallographic parameters, including the unit cell volume and theoretical density, were determined using CrystalMaker software based on the reported crystal structure. The crystallographic model employed for these calculations is consistent with that reported by Grendal et al. [27], which provides a reliable structural framework for tetragonal tungsten bronze compounds.

A clear influence of assisted sintering temperature on crystallinity is observed. The samples sintered at 500 °C generally exhibit sharper and more intense diffraction peaks compared with the 400 °C series, indicating improved crystallinity, enhanced atomic ordering, and possible grain growth at higher sintering temperatures. Such enhancement in diffraction intensity is commonly associated with improved structural ordering and reduced lattice imperfections during thermal treatment [15, 28–30].

The influence of sodium substitution becomes increasingly evident with increasing dopant concentration. In both the T1 and T2 series, the diffraction peak intensity around 28–29° gradually decreases with increasing Na content, particularly for the BKGF-3N compositions. In addition, slight peak shifts are observed in highly doped samples, suggesting successful incorporation of Na^+ ions into the TTB lattice and corresponding lattice distortion due to ionic substitution. The smaller ionic radius of Na^+ compared with K^+ within the A-site of the TTB framework introduces localized lattice distortion, preserving the tetragonal structure while producing subtle modifications in lattice strain. Similar behavior has been reported for alkali-modified TTB ceramics [15, 31–34].

The effect of ionic aqueous medium treatment is also reflected in the diffraction behavior. Certain salt-assisted samples, particularly BKGF-2NST$_1$, exhibit comparatively reduced peak intensity, suggesting that the combined influence of sodium substitution and ionic transient liquid processing may introduce localized structural disorder or defect formation. Although assisted ionic processing can enhance densification, excessive ionic incorporation may simultaneously influence crystallinity and defect equilibria within the TTB framework.

Particle size analysis presented in Figure 3 reveals that the average particle size increases progressively with sodium concentration, ranging from approximately 2.98 μm for undoped compositions to nearly 7.37 μm for the highly doped BKGF-3N samples.

Generally, smaller particles are expected to promote densification due to their higher surface energy and

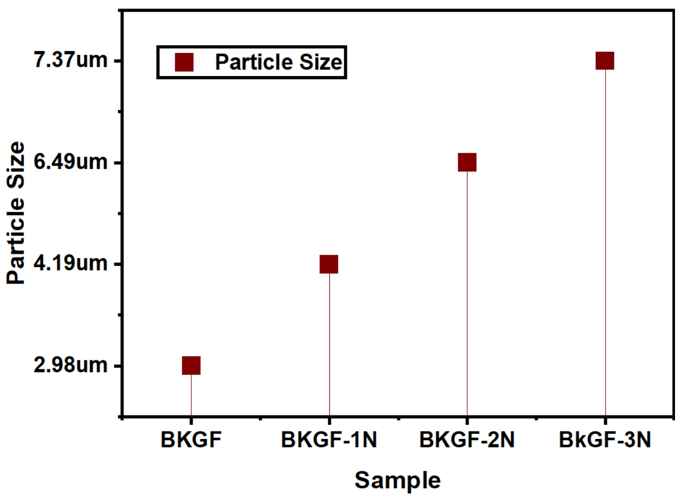

Figure 3. Particle size analysis of $BaK_{1-x}Na_xGd_3Fe_5O_{15}$ compositions with varying sodium concentration.

shorter diffusion pathways during sintering [35]. However, the density results summarized in Table 1 indicate that densification behavior is strongly influenced not only by particle size, but also by dopant concentration, ionic medium treatment, and assisted sintering temperature.

Table 1. Relative Density of $BaK_{1-x}Na_xGd_3Fe_5O_{15}$ processed under different assisted sintering and ionic medium conditions.

Sample	Bulk Density (g/cm^3)	Theoretical Density (g/cm^3)	Relative Density (%)
BKGF-T1	3.96	4.21	94.1
BKGF-ST1	3.70	4.21	87.9
BKGF-T2	3.44	4.21	81.7
BKGF-ST2	3.85	4.21	91.4
BKGF-1NT1	3.89	4.39	88.6
BKGF-1NST1	3.47	4.39	79.0
BKGF-1NT2	3.54	4.39	80.6
BKGF-1NST2	4.32	4.39	98.4
BKGF-2NT1	3.46	4.45	77.8
BKGF-2NST1	3.81	4.45	85.6
BKGF-2NT2	3.81	4.45	85.6
BKGF-2NST2	3.79	4.45	85.2
BKGF-3NT1	3.79	4.46	85.0
BKGF-3NST1	3.81	4.46	85.4
BKGF-3NT2	3.46	4.46	77.6
BKGF-3NST2	3.81	4.46	85.4

Table 1 presents the bulk, theoretical and relative densities of $BaK_{1-x}Na_xGd_3Fe_5O_{15}$ ceramics processed under different assisted sintering conditions and ionic medium conditions. For the 400 °C (T_1) series, the bulk density decreases with increasing Na substitution from 3.96 g/cm^3 (94.1%) for BKGF-T_1 to 3.89 g/cm^3 (88.6%) for BKGF-1NT1 and reaches a minimum of 3.46 g/cm^3 (77.8%) for BKGF-2NT_1, followed by an increase to 3.79 g/cm^3 (85.0%) for BKGF-3NT_1. In the 500 °C (T_2) series, a marked variation is observed, with BKGF-1NST_2 exhibiting the highest bulk density of 4.32 g/cm^3 and a relative density of 98.4%, compared with 3.54 g/cm^3 and 80.6% for the corresponding BKGF-1NT_2 sample. Among all compositions and processing conditions, BKGF-1NST2 shows the highest densification, whereas BKGF-2NT_1 exhibits the lowest relative density (77.8%). These results indicate that the densification behavior is strongly influenced by both Na substitution level and processing route, which enhances mass transport, grain boundary diffusion, and particle rearrangement during assisted sintering [16, 19, 22].

The observed differences between deionized water processed and salt-assisted samples further demonstrate the important role of transient liquid chemistry in the densification and structural evolution of the ceramics. The presence of dissolved ionic species in the transient medium likely promotes localized mass transport and pore filling, resulting in improved grain connectivity and reduced residual porosity in selected compositions. However, excessive ionic incorporation may also contribute to local structural disorder and defect formation, which can influence diffraction intensity and functional behavior. These competing effects suggest that transient liquid chemistry strongly affects crystallinity, densification, dielectric relaxation, and magnetic interactions in cold-assisted sintered TTB ceramics.

The frequency-dependent dielectric behavior of $BaK_{1-x}Na_xGd_3Fe_5O_{15}$ ceramics is presented in Figures 4 and 5, showing the variation of relative permittivity (ε_r) and dielectric loss tangent ($\tan\delta$) as a function of sodium concentrations, salt-assisted processing, and assisted sintering temperature (T_1 = 400 °C and T_2 = 500 °C). All compositions exhibit pronounced frequency dependent dielectric behavior, which is characteristic of tetragonal tungsten bronze (TTB) ceramics.

The relative permittivity generally decreases with increasing frequency, particularly below ~1 MHz, due to the gradual reduction in the contribution of space-charge, interfacial, dipolar, and grain boundary polarization mechanisms. At lower frequencies, charge carriers and defect dipoles can readily follow the applied alternating electric field, resulting in higher polarization and consequently higher dielectric permittivity. As the frequency increases, these polarization mechanisms become progressively unable

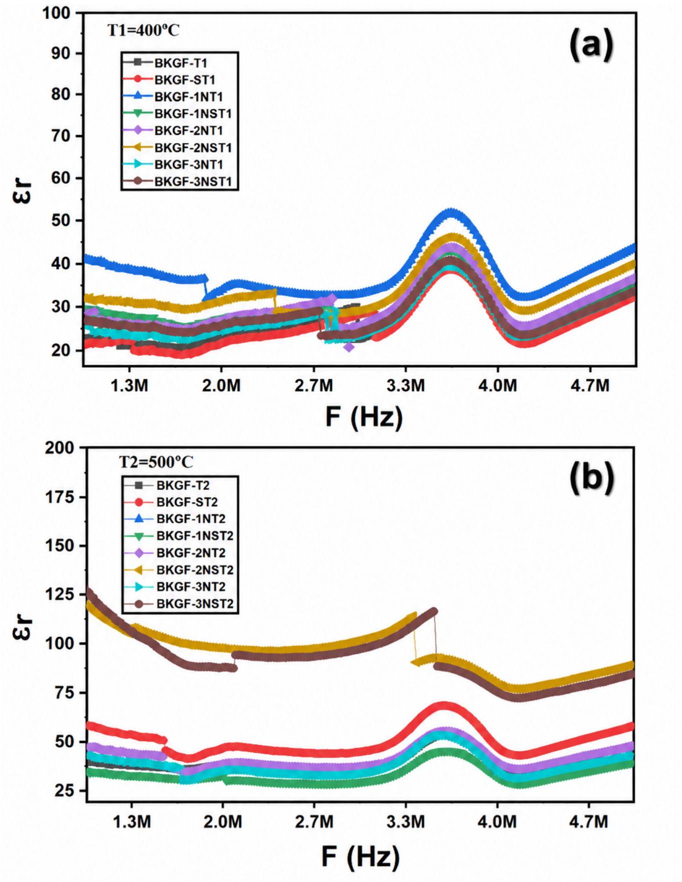

Figure 4. Relative permittivity (ε_r) of $BaK_{1-x}Na_xGd_3Fe_5O_{15}$ from 1 MHz to 5 MHz ($x = 0.10$, 0.20, 0.30). (a) At $T = 400\,°C$; (b) At $T = 500\,°C$.

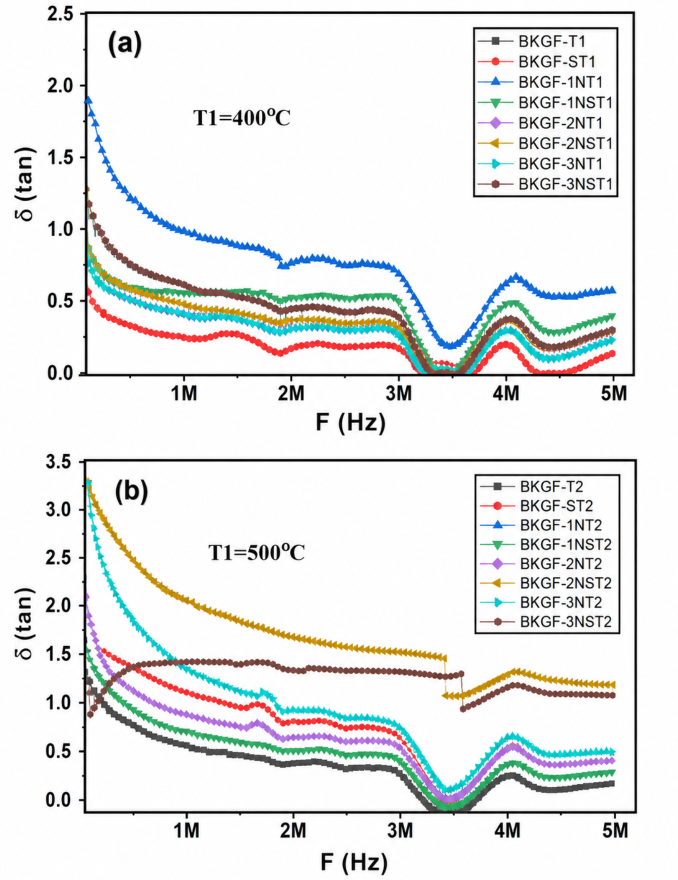

Figure 5. Dielectric losses ($\tan\delta$) of $BaK_{1-x}Na_xGd_3Fe_5O_{15}$ from 1 MHz to 5 MHz ($x = 0.10, 0.20, 0.30$). (a) At $T = 400\,°C$; (b) At $T = 500\,°C$.

to respond to the rapidly alternating electric field, leading to reduction in the dielectric constant. Similar frequency dependent dielectric dispersion has been reported for iron-containing oxide ceramics and TTB systems [15, 31]. Among these compositions, BKGF-2NST$_2$ assisted-sintered at 500 °C exhibited the highest relative permittivity (∼130–135) at 1 MHz, whereas BKGF-1NT$_1$ showed the highest permittivity (∼50–52) in the 400 °C series. This indicates that both Na^+ substitution and assisted sintering temperature influence the dielectric response.

The observed dielectric relaxation behavior can be interpreted using the Maxwell–Wagner interfacial polarization model together with Koop's phenomenological theory [36, 37]. According to this model, the ceramic microstructure consists of relatively conductive grains separated by highly resistive grain boundaries. At lower frequencies, charge carriers accumulate at the grain boundaries, producing significant space-charge polarization and consequently higher dielectric permittivity. As the applied frequency increases, the accumulated charges become unable to follow the alternating electric field, resulting in a gradual decrease in dielectric constant. Similar dielectric relaxation behavior governed by interfacial polarization has been reported for substituted multifunctional oxide ceramics [38].

In addition to interfacial polarization, the dielectric behavior may also be influenced by defect chemistry. Oxygen vacancies generated during ceramic processing are likely to act as localized charge-trapping centers, while partial substitution of K^+ with Na^+ may introduce local lattice distortion and modify charge compensation behavior within the TTB framework. Furthermore, localized Fe^{2+}/Fe^{3+} electron hopping may contribute to short range charge transport and dielectric relaxation. These mechanisms are consistent with the dielectric behavior reported for substituted oxide ceramics in the literature [37, 38].

The dielectric loss tangent ($\tan\delta$) also decreases significantly with increasing frequency for most compositions, indicating reduced energy dissipation at higher frequencies. The comparatively high dielectric losses observed at lower frequencies may be associated with Maxwell–Wagner interfacial polarization, electrode polarization, and charge accumulation at grain boundaries and defect-rich interfaces. The reduction in dielectric loss observed around 3.5–4 MHz is consistent with dielectric relaxation processes associated with defect-mediated and interfacial polarization mechanisms. Among the investigated samples, BKGF-ST_1 exhibited the lowest dielectric loss within the measured frequency range after salt-assisted processing, indicating improved dielectric stability.

The assisted sintering temperature strongly influences the dielectric response of the ceramics. Samples sintered at 400 °C (T_1 series) generally exhibit lower dielectric losses than those sintered at 500 °C (T_2 series), particularly at lower frequencies. Although higher assisted sintering temperatures improve crystallinity and structural ordering, they may also modify grain boundary resistance and defect concentration, thereby influencing dielectric loss and polarization behavior. Consequently, variations in dielectric loss among different compositions may result from changes in defect chemistry and charge transport associated with the assisted sintering temperature.

The influence of sodium substitution and salt-assisted processing is strongly composition dependent. In the T_1 series, the salt-assisted composition BKGF-ST_1 exhibits comparatively lower dielectric loss, indicating improved dielectric stability and reduced energy dissipation. In contrast, the BKGF-$2NT_2$ and BKGF-$2NST_2$ samples in the T_2 series exhibit comparatively higher dielectric losses, which may be associated with changes in defect concentration, grain boundary resistance, and localized Fe^{2+}/Fe^{3+} hopping induced by the higher assisted sintering temperature.

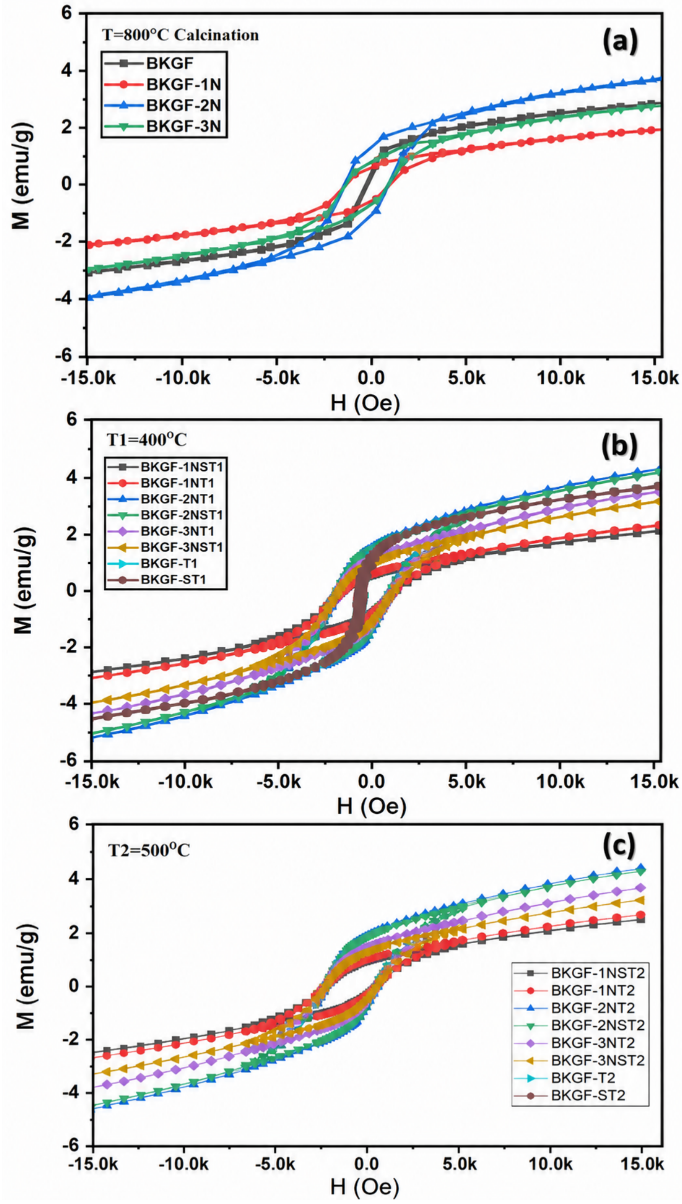

Figure 6. Hysteresis loops of $BaK_{1-x}Na_xGd_3Fe_5O_{15}$ ($x = 0.10, 0.20, 0.30$) samples. (a) Calcined powder; (b) CS at 150 °C + AS at 400 °C; (c) CS at 150 °C + AS at 500 °C.

Although increased density generally improves particle packing and reduces residual porosity, the results indicate that densification alone does not determine the dielectric response of $BaK_{1-x}Na_xGd_3Fe_5O_{15}$ ceramics. BKGF-$1NST_2$ exhibited the highest bulk density but did not show the highest dielectric constant. This observation suggests that dielectric behavior is additionally influenced by crystallinity, grain-boundary characteristics, defect chemistry, oxygen-vacancy concentration, and localized Fe^{2+}/Fe^{3+} hopping rather than by densification alone.

The magnetic properties of $BaK_{1-x}Na_xGd_3Fe_5O_{15}$ ceramics were investigated using vibrating sample magnetometry (VSM), and the corresponding M–H hysteresis loops are presented in Figure 6, while the magnetic parameters including saturation magnetization (M_s), remanent magnetization (M_r), and coercivity (H_c) are summarized in Table 2. All compositions exhibit clear hysteresis loops, confirming ferromagnetic/ferrimagnetic behavior at room temperature due to Fe^{3+}-mediated magnetic interactions within the tetragonal tungsten bronze (TTB) framework [10, 39–41].

As observed in Figure 6(b, c), assisted sintering at 500 °C generally enhances the magnetic response compared with the 400 °C series. The T2 samples generally exhibit comparable or moderately varied

Table 2. H_c, M_r, M_s values of $BaK_{1-x}Na_xGd_3Fe_5O_{15}$ ($x = 0.00, 0.10, 0.20, 0.30$) ceramics.

Temperature	Sample	M_s (emu/g)	M_r (emu/g)	H_c (Oe)
Sintered T_1 (400 °C)	BKGF-T1	4.38	0.544	151.428
	BKGF-ST1	4.36	0.538	147.588
	BKGF-1NST1	2.73	0.696	1384.611
	BKGF-1NT1	2.92	0.745	1345.312
	BKGF-2NT1	5.04	1.55	1417.268
	BKGF-2NST1	4.87	1.50	1430.209
	BKGF-3NT1	4.19	1.24	1465.517
	BKGF-3NST1	3.81	1.12	1474.592
Sintered T_2 (500 °C)	BKGF-T2	4.92	0.536	143.745
	BKGF-ST2	5.01	0.553	146.505
	BKGF-1NST2	2.81	0.731	1377.925
	BKGF-1NT2	3.04	0.783	1409.759
	BKGF-2NT2	4.97	1.59	1435.843
	BKGF-2NST2	4.83	1.54	1408.431
	BKGF-3NT2	4.14	1.23	1404.644
	BKGF-3NST2	3.66	1.05	1410.269

M_s, M_r, and H_c values relative to the T1 series, with composition-dependent trends reflecting the interplay between improved crystallinity and modified defect chemistry at higher assisted sintering temperatures. Similar improvements in magnetic behavior after cold-assisted sintering have also been reported in related TTB ceramics processed through low-temperature routes [14, 22]. The effect of sodium substitution is particularly significant in modifying coercivity and remanent magnetization. As summarized in Table 2, the undoped compositions BKGF-T_1/T_2 and BKGF-ST_1/ST_2 exhibit low coercivity values (∼150 Oe), characteristic of soft magnetic behavior. In contrast, sodium-doped samples show a substantial increase in coercivity, ranging from approximately 1345 to 1475 Oe, indicating enhanced magnetic anisotropy and stronger domain wall pinning. Among all investigated compositions, the BKGF-2NT_1 and BKGF-2NT_2 samples exhibit the highest magnetic performance, with M_s values of approximately 5 emu/g and coercivity exceeding 1400 Oe. For $x = 0.20$, the enhanced magnetic performance observed suggests an optimum balance between defect concentration and structural ordering. Additional lattice distortion may be introduced due to excessive Na substitution ($x = 0.30$) that weakens long-range magnetic exchange interactions despite improved crystallinity, consistent with observations in other substituted oxide systems [40, 42]. This suggests that the intermediate sodium concentration optimizes magnetic exchange interactions and magnetic domain stability within the TTB lattice.

The 2N sodium concentration appears to optimize this magnetically hard behavior, characterized by enhanced coercivity, likely by influencing the distribution of magnetic ions or promoting optimal magnetic domain formation. Conversely, salt-assisted processing generally results in slightly lower saturation magnetization compared to the corresponding NT samples, suggesting a modest reducing effect on the overall magnetic moment. This complex interplay of dopants and processing conditions allows for modification of the magnetic characteristics, which is crucial for potential multiferroic applications.

The present study focuses on the structural, dielectric, and magnetic properties of $BaK_{1-x}Na_xGd_3Fe_5O_{15}$ ceramics processed by cold-assisted sintering. Although X-ray diffraction and density measurements provide evidence of phase formation, crystallinity, and densification, detailed microstructural characteristics such as grain morphology, grain size, and pore distribution could not be directly examined because SEM analysis was beyond the scope of the present work. Future investigations will include SEM characterization to establish a direct correlation between the microstructure and the observed dielectric and magnetic properties.

4 Conclusion

$BaK_{1-x}Na_xGd_3Fe_5O_{15}$ tetragonal tungsten bronze ceramics were successfully synthesized by a cold-assisted sintering route followed by assisted sintering at 400 °C and 500 °C. XRD analysis confirmed the formation of the TTB phase, while assisted sintering improved the crystallinity and densification of the ceramics. BKGF-1NST_2 exhibited the highest bulk density of 4.32 g/cm^3. Dielectric measurements revealed the characteristic frequency-dependent response of TTB ceramics, with the BKGF-2NST$_2$ exhibiting the highest relative permittivity (approximately 130–135 at ~1 MHz), whereas the salt-assisted BKGF-ST$_1$ showed the lowest dielectric loss within the investigated frequency range. Magnetic measurements confirmed ferrimagnetic behavior for all compositions, with the BKGF-2NT$_2$ demonstrating optimal overall magnetic performance, including saturation magnetization ($M_s = 4.97$ emu/g), remanent magnetization ($M_r = 1.59$ emu/g), and coercivity ($H_c = 1435.84$ Oe), attributed to optimized magnetic exchange interactions and improved grain connectivity at 500 °C assisted sintering. Overall, the combined effects of Na$^+$ substitution and assisted sintering provide an effective strategy for optimizing the structural, dielectric, and magnetic properties of $BaK_{1-x}Na_xGd_3Fe_5O_{15}$ ceramics through a low-temperature processing route.

Data Availability Statement

Data will be made available on request.

Funding

This work was supported by the Higher Education Commission of Pakistan under Grant NRPU-17049.

Conflicts of Interest

Fayaz Hussain served as an Associate Editor of the *Journal of Advanced Electronic Materials* at the time of manuscript submission. To ensure the integrity of the peer-review process, Fayaz Hussain was not involved in the editorial handling, peer review, or decision-making process for this manuscript, which was handled independently by another editor. The remaining authors declare no conflicts of interest.

AI Use Statement

The authors declare that no generative AI was used in the preparation of this manuscript.

Ethical Approval and Consent to Participate

Not applicable.

References

[1] Khomskii, D. I. (2006). Multiferroics: Different ways to combine magnetism and ferroelectricity. *Journal of Magnetism and Magnetic Materials, 306*(1), 1–8. [CrossRef]

[2] Roulland, F., Josse, M., Castel, E., & Maglione, M. (2009). Influence of ceramic process and Eu content on the composite multiferroic properties of the Ba6-2xLn2xFe1+ xNb9-xO30 TTB system. *Solid state sciences, 11*(9), 1709-1716. [CrossRef]

[3] Spaldin, N. A., & Fiebig, M. (2005). The renaissance of magnetoelectric multiferroics. *Science, 309*(5733), 391-392. [CrossRef]

[4] Fiebig, M. (2005). Revival of the magnetoelectric effect. *Journal of physics D: applied physics, 38*(8), R123-R152. [CrossRef]

[5] Josse, M., Bidault, O., Roulland, F., Castel, E., Simon, A., Michau, D., ... & Maglione, M. (2009). The Ba2LnFeNb4O15 "tetragonal tungsten bronze": Towards RT composite multiferroics. *Solid state sciences, 11*(6), 1118-1123. [CrossRef]

[6] Schmid, H. (1994). Multi-ferroic magnetoelectrics. *Ferroelectrics, 162*(1), 317-338. [CrossRef]

[7] Wang, D. H., Goh, W. C., Ning, M., & Ong, C. K. (2006). Effect of Ba doping on magnetic, ferroelectric, and magnetoelectric properties in mutiferroic BiFeO3 at room temperature. *Applied physics letters, 88*(21). [CrossRef]

[8] Aamlid, S. S., Selbach, S. M., & Grande, T. (2019). The effect of cation disorder on ferroelectric properties of SrxBa1-xNb2O6 tungsten bronzes. *Materials, 12*(7), 1156. [CrossRef]

[9] Schneck, J., Toledano, J. C., Joffrin, C., Aubree, J., Joukoff, B., & Gabelotaud, A. (1982). Neutron scattering study of the tetragonal-to-incommensurate ferroelastic transition in barium sodium niobate. *Physical Review B, 25*(3), 1766. [CrossRef]

[10] Fang, P. H., & Roth, R. S. (1960). Ferroelectric and ferrimagnetic properties of (Ba6-2xR2x)(Nb9-xFe1+x) O30. *Journal of Applied Physics, 31*(5), S278-S278. [CrossRef]

[11] Wang, D., Hussain, F., Khesro, A., Feteira, A., Tian, Y., Zhao, Q., & Reaney, I. M. (2017). Composition and temperature dependence of structure and piezoelectricity in (1-x)(K1-yNay) NbO3-x (Bi1/2Na1/2) ZrO3 lead-free ceramics. *Journal of the American Ceramic Society, 100*(2), 627-637. [CrossRef]

[12] Han, M., Wang, Y., Tong, Y., Feng, Z., Chao, X., Yang, Z., ... & Wei, L. (2025). Remarkable energy storage performances in tungsten bronze Sr2Ag0. 2Na0. 8Nb5O15-based ceramics through relaxor tuning. *Chemical Engineering Journal, 513*, 162844. [CrossRef]

[13] Fan, J., Yang, B., Wei, L., & Wang, Z. (2016). B-cation effect on relaxor behavior and electric properties in Sr2NaNb5-xSbxO15 tungsten bronze ceramics. *Ceramics International, 42*(3), 4054-4062. [CrossRef]

[14] Fatima, S. M., Hussain, F., Tabak, Y., Riaz, M. F., Yıldız, İ., Evcin, A., ... & Almuhawish, N. F. (2026). Cold-Sintered K 3 Bi 3-x Na x Mg 2 Fe 5-x Nb x O 15 Tetragonal Tungsten Bronze Ceramics: Structure,

Dielectric, and Magnetic Properties. *Journal of Alloys and Compounds*, 187476. [CrossRef]

[15] Jindal, S., Vasishth, A., Devi, S., Aggarwal, N., & Kushwah, K. K. (2020). Investigation of structural, ferroelectric and magnetic properties of iron doped tungsten bronze multiferroic ceramics. *Physica B: Condensed Matter, 595*, 412341. [CrossRef]

[16] Grasso, S., Biesuz, M., Zoli, L., Taveri, G., Duff, A. I., Ke, D., ... & Reece, M. J. (2020). A review of cold sintering processes. *Advances in Applied Ceramics, 119*(3), 115-143. [CrossRef]

[17] Ibn-Mohammed, T., Randall, C. A., Mustapha, K. B., Guo, J., Walker, J., Berbano, S., ... & Reaney, I. M. (2019). Decarbonising ceramic manufacturing: A techno-economic analysis of energy efficient sintering technologies in the functional materials sector. *Journal of the European ceramic society, 39*(16), 5213-5235. [CrossRef]

[18] Faouri, S. S., Mostaed, A., Dean, J. S., Wang, D., Sinclair, D. C., Zhang, S., ... & Reaney, I. M. (2019). High quality factor cold sintered Li2MoO4BaFe12O19 composites for microwave applications. *Acta Materialia, 166*, 202-207. [CrossRef]

[19] Guo, J., Floyd, R., Lowum, S., Maria, J. P., Herisson de Beauvoir, T., Seo, J. H., & Randall, C. A. (2019). Cold sintering: progress, challenges, and future opportunities. *Annual Review of Materials Research, 49*(1), 275-295. [CrossRef]

[20] Heidary, D. S. B., Lanagan, M., & Randall, C. A. (2018). Contrasting energy efficiency in various ceramic sintering processes. *Journal of the European Ceramic Society, 38*(4), 1018-1029. [CrossRef]

[21] Lan, J. J., Chen, X. M., Liu, L. N., Lian, H. L., He, Y. R., Song, Y. C., ... & Liu, P. (2023). Low-temperature synthesis of K0. 5Na0. 5NbO3 ceramics in a wide temperature window via cold-sintering assisted sintering method and enhanced electrical properties. *Journal of the European Ceramic Society, 43*(1), 73-81. [CrossRef]

[22] Zubairi, H., Hussain, F., Sheikh, S., Shaikh, A. A., Wang, D., & Reaney, I. M. (2023). Comparative study of cold assisted and conventional sintering of (1-2x) K0. 5Na0. 5NbO3-xBaTiO3-xBiFeO3 multiferroic ceramics. *Materials Science and Engineering: B, 296*, 116632. [CrossRef]

[23] Cong, L., Huajing, W., Jianzhang, M., Baoyu, D., Xiao, W., Tengfei, L., ... & Xing, Y. (2020). Effect of dwell time on cold sintering assisted sintering based highly transparent 0.9 K0. 5Na0. 5NbO3-0.1 LiBiO3 ceramics. *Journal of Alloys and Compounds, 826*, 154249. [CrossRef]

[24] Ma, J., Li, H., Wang, H., Lin, C., Wu, X., Lin, T., ... & Yu, X. (2019). Composition, microstructure and electrical properties of K0. 5Na0. 5NbO3 ceramics fabricated by cold sintering assisted sintering. *Journal of the European Ceramic Society, 39*(4), 986-993. [CrossRef]

[25] Bartoletti, A., Mercadelli, E., Gondolini, A., & Sanson, A. (2024). Exploring the potential of cold sintering for proton-conducting ceramics: A review. *Materials, 17*(20), 5116. [CrossRef]

[26] Jamieson, P. B., Abrahams, S. C., & Bernstein, J. L. (1969). Ferroelectric tungsten bronze-type crystal structures. II. Barium sodium niobate Ba (4+x) Na (2-2x) Nb10O30. *The Journal of Chemical Physics, 50*(10), 4352-4363. [CrossRef]

[27] Grendal, O. G., Evans, D. M., & Aamlid, S. S. (2023). Revisiting the structures and phase transitions of Ba2NaNb5O15. *Applied Crystallography, 56*(5), 1456-1465. [CrossRef]

[28] Peirson, H., Pan, J., Li, Y., Hall, D. A., Brown, A. P., Drummond-Brydson, R. M., & Milne, S. J. (2023). Structure and dielectric properties of yttrium-doped Ca0. 28Ba0. 72Nb2O6 ceramics. *Journal of Alloys and Compounds, 950*, 169891. [CrossRef]

[29] Gardner, J., & Morrison, F. D. (2014). A-site size effect in a family of unfilled ferroelectric tetragonal tungsten bronzes: Ba4R0. 67Nb10O30 (R= La, Nd, Sm, Gd, Dy and Y). *Dalton transactions, 43*(30), 11687-11695. [CrossRef]

[30] Rahaman, M. N. (2017). *Ceramic processing and sintering*. CRC press. [CrossRef]

[31] Bendahhou, A., Jalafi, I., Chaou, F., Barkany, S. E., Bahari, Z., & Abou-Salama, M. (2023). Effect of sodium substitution by yttrium on the structural, dielectric and electrical properties of Ba2Na (1-3x) YxNb5O15 ceramics. *Heliyon, 9*(11). [CrossRef]

[32] Li, R., Pu, Y., Zhang, Q., Wang, W., Li, J., Du, X., ... & Sun, Z. (2020). The relationship between enhanced dielectric property and structural distortion in Ca doped Ba2NaNb5O15 tungsten bronze ceramics. *Journal of the European Ceramic Society, 40*(13), 4509-4516. [CrossRef]

[33] Miller, A. J., Rotaru, A., Arnold, D. C., & Morrison, F. D. (2015). Effect of local A-site strain on dipole stability in A6GaNb9O30 (A= Ba, Sr, Ca) tetragonal tungsten bronze relaxor dielectrics. *Dalton Transactions, 44*(23), 10738-10745. [CrossRef]

[34] Zhang, X., Yan, H., & Reece, M. J. (2008). Effect of A site substitution on the properties of CaBi2Nb2O9 ferroelectric ceramics. *Journal of the American Ceramic Society, 91*(9), 2928-2932. [CrossRef]

[35] Rahaman, M. N. (2017). *Ceramic Processing*. CRC Press. [CrossRef]

[36] Koops, C. G. (1951). On the Dispersion of Resistivity and Dielectric Constant of Some Semiconductors at Audiofrequencies. *Physical Review, 83*(1), 121–124. [CrossRef]

[37] Mandve, D. N., & Waghule, N. N. (2026). Structural, Dielectric, Magnetic, and Magnetoelectric Properties of Lead-Free BCZT–CZFO Composite Ceramics. *Journal of Superconductivity and Novel Magnetism, 39*(4), 117. [CrossRef]

[38] Ali, A., Safeen, K., Alrefaee, S. H., Alhodaib, A., Safeen, A., Saydaxmetova, S., ... & Zaman, A. (2025). Studies of structural, optical, magnetic and dielectric properties of Sr0. 7Bi0. 2 (Ti1-xZrx) O3 0.0$\leq$ x $\leq$ 0.6 ceramics for wireless application. *Electrochemistry Communications*, *176*, 107962. [CrossRef]

[39] Givord, D. (2001). Introduction to Magnetism and Magnetic Materials. In *Magnetism and Synchrotron Radiation* (pp. 3–23). Springer. [CrossRef]

[40] El-Hilo, M., Pfeiffer, H., O'grady, K., Schüppel, W., Sinn, E., Görnert, P., ... & Chantrell, R. W. (1994). Magnetic properties of barium hexaferrite powders. *Journal of magnetism and magnetic materials*, *129*(2-3), 339-347. [CrossRef]

[41] FRS, E. C. S. (1947). Ferromagnetism. *Reports on Progress in Physics*, *11*(1), 43-112. [CrossRef]

[42] Shah, W. H., Safeen, K., & Rehman, G. (2012). Effects of divalent alkaline earth ions on the magnetic and transport features of La0. 65A0. 35Mn0. 95Fe0. 05O3 (A= Ca, Sr, Pb, Ba) compounds. *Current Applied Physics*, *12*(3), 742-747. [CrossRef]

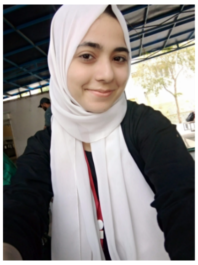

Syeda Mahnoor Fatima received the M.E. degree in Materials Engineering from NED University of Engineering and Technology, Karachi, Pakistan, in 2024. She is currently working as a Research Assistant in the Department of Materials Engineering at NED University of Engineering and Technology, Pakistan. Her research interests include functional ceramics, dielectric and magnetic materials, and advanced sintering techniques. (Email: fatimamahnoor923@gmail.com)

Fayaz Hussain is currently serving as Professor & Chairman of the Department of Materials Engineering at NED University of Engineering and Technology, Karachi, Pakistan. He is an Editorial Board Member of several prestigious journals, including *Ceramics* (JCR), *International Journal of Energy Research*, *Frontiers in Materials* (JCR), *Electro-active Materials* (Malaysia), *Journal of Advanced Dielectrics* (Xian Jiaotong University, China), and *Crystals* (JCR). (Email: fhussain@neduet.edu.pk)

Shehreen Nadeem received the M.E. degree from the Department of Materials Engineering, NED University of Engineering and Technology, University Road, Karachi 75270, Pakistan. (Email: shehrinnadeem16@gmail.com)

Muhammad Fahad Riaz received his Ph.D. degree in Materials Engineering from NED University of Engineering and Technology, Karachi, Pakistan, and Harbin Institute of Technology (HIT), China. His research interests include dielectric materials, energy storage devices, and multi-layer ceramic capacitors (MLCCs). (Email: Fahad.riaz@duet.edu.pk)

Sajida Sheikh is an Assistant Professor in the Department of Materials Engineering at NED University of Engineering and Technology, University Road, Karachi 75270, Pakistan. (Email: sajidashiekh@neduet.edu.pk)

Yasemin Tabak is with TUBITAK National Metrology Institute (UME), Gebze, Kocaeli 41470, Türkiye. (Email: yasemin.tabak@tubitak.gov.tr)

Atilla Evcin is with the Department of Materials Science and Engineering, Afyon Kocatepe University, Afyonkarahisar 032004, Türkiye. (Email: evcin@aku.edu.tr)